Perforation of sandwich plates with graded hollow sphere cores under impact loading

Huabin Zeng, Stephane Pattofatto, Han Zhao, Yannick Girard, Valia Fascio

Perforation of sandwich plates with graded hollow sphere cores under impact loading

H.B.Zeng[a], S.Pattofatto[a], H.Zhao[a,*], Y.Girard[b] and V.Fascio[c]

[a]Laboratoire de Mécanique et Technologie,
ENS Cachan/CNRS UMR8535/UPMC/PRES UniverSud Paris,
61, Avenue du président wilson, 94235 Cachan cedex,

[b]EADS CCR, quai Marcel Dassault – BP 76
92152 Suresnes Cedex, France

[c]ATECA/Advanced Materials & Systems (AMS) Verlhaguet,
82000 MONTAUBAN, France

Abstract

In this paper, sandwich plates made from 0.8mm 2024 T3 aluminium alloy skin sheets and graded polymeric hollow sphere cores (having various density gradients) are studied. The experiments at 45m/s were performed with an inversed perforation setup using SHPB system. Quasi-static tests using the same clamping system allow for the rate effect investigation. Numerical simulations are performed in order to get the indispensable local information (which is not experimentally available) to better understand the perforation process.

With these experimental and numerical tools, it is found that the gradient profiles change the perforation process under studied impact loading, whereas they have no influence under quasi-static loading. Under impact loading, a competition of two deforming scenarios at the early stage governed the whole process afterwards. One is the global crush of the first layer in contact with the incident skin and the other is the piercing of the incident skin sheet. When the first layer is rather strong, the incident skin sheet breaks and the perforator makes a hole in the core afterwards. When the first layer is rather weak, the skin sheet folds into the core and develops a much more energy consuming process. The best gradient profile in terms of the energy absorption capacity as well as the non-sheet breaking criterion should be a lower first layer and a progressively enhanced core.

* Please address all the correspondence to zhao@lmt.ens-cachan.fr

1. Introduction

The impact behaviours (energy absorption, perforation limits) are the important design features for sandwich panels used in aeronautics structures. For example, such panels are used to protect the airplane cockpit against bird strikes [1,2]. The core materials of such panels (honeycombs, foams, hollow sphere agglomerates, etc.) play often dominant roles in the whole energy absorption as well as their penetration behaviour.

With the development of functionally graded materials (FGMs) introduced in the materials sciences over the last decade, the core materials with graded properties can be nowadays made by different manufacturing techniques [3]. Important achievements have also been made in order to understand the mechanical response of FGMs submitted to impact loadings. Li et al. [4] have investigated the impulsive loading in the layered and graded structures using numerical models. Gupta [5] has studied a functionally graded syntactic foam material (FGSF). Apetre et al. [6] studied the low-velocity impact response of sandwich beams with functionally graded core. All those works, even mostly based on the theoretical analyses and the numerical simulations, show that the introduction of a property gradient will largely modify the overall response of the designed FGM structures.

This paper deals with the behaviour of sandwich plates with graded core materials under impact penetrating loads. The studied sandwich specimens are made from aluminium skin sheets and polymeric hollow sphere agglomerates with various density gradient profiles. Perforation behaviour under static and dynamic loading (performed using newly developed inversed perforation test with a Hopkinson pressure bar) is measured. A significant influence of the property gradient is observed. Numerical simulations of all these tests provide an interesting explanation about how the property gradient has been involved in the perforation scheme of sandwich plates.

2. Sandwich specimens and testing methods

2.1 The sandwich specimen

Hollow sphere agglomerates made by bounding or sintering have not only good mechanical properties such as high specific energy absorption capacities and high specific strengths, but also excellent thermal and acoustic properties [7].

The studied hollow sphere agglomerates have been manufactured and supplied by ATECA. The replication process is used to produce polyepoxide hollow spheres of specified external diameter around 2.5 mm. The thickness of hollow spheres is controlled in order to

vary their density and the subsequent strength [8]. The supplied hollow sphere agglomerates are randomly packed and joined by sintering, which is a packing mode corresponding to the industrial mass production acquirement.

The cylindrical sandwich specimens (60 mm diameter) are made of two 0.8 mm skin sheets of 2024 T3 aluminium alloy and a core of 40 mm thick. The first four types of samples as listed in table 1 are made with homogeneous polymeric hollow sphere cores of different densities varying from 156 to 468kg/m3. The last two sample types S-A4321 and S-B1234 concern the cores with density gradient, which is obtained by changing hollow sphere density every 10mm. Their density profiles are all linear ones (figure 1).

Sandwich	Core density (kg/m^3)
S-C1	156
S-C2	242
S-C3	343
S-C4	468
S-A4321	302
S-B1234	302

Table 1: Core density of the specimens

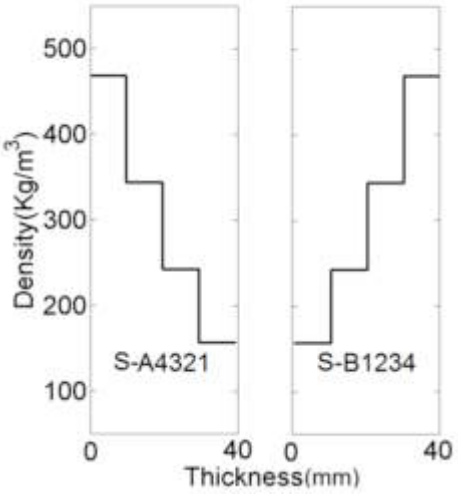

Figure 1: The graded profile of the S-A4321 and S-B1234 sandwich plates

It is interesting to notice that the density gradient is obtained only with the change of the thickness of hollow spheres. Thus, the thermal and acoustical properties (depending only on the packing and external diameters of the hollow sphere) will not change with the density profile. The photograph of the sandwich samples with homogeneous core (a) and graded core (b) shown in Figure 2 do not reveal any geometric difference.

(a) (b)

Figure 2 The Photograph of sandwich sample with homogeneous core (a) and graded core (b)

2.2 Experimental setup

Experimental studies on sandwich panels have been reported in previous works [9-13]. In this paper, the inversed perforation method with Hopkinson pressure bars is adopted to study sandwich samples under impact loading [14]. It consists of launching a sandwich sample against a long instrumented Hopkinson bar. The main advantage of such a setup lies in an accurate force measurement during the whole perforation process. The proposed inversed perforation testing set-up uses a gas gun with a 70 mm inner diameter barrel and a 16mm diameter and 6-m-long rod with a semi-spherical nose at its perforating end. Figure 3 shows an outline of the experimental set-up.

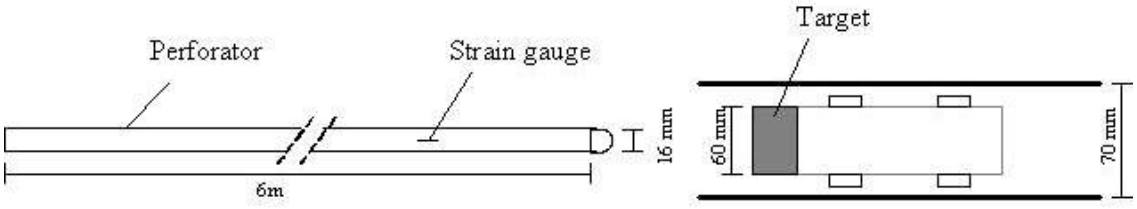

Figure 3 Experimental set-up for the inversed perforation test

The target sandwich sample is launched with the aid of a hollow tube-like projectile, which is made from an aluminium tube with a welded bottom plate at one end. Two Teflon rings are screwed on the tube which allow for a small friction between projectile and the

barrel of the gas gun. The circular sandwich samples are mounted between the open end of the tube-like projectile and an aluminium-clamping ring. The fixture is realized by six uniformly distributed bolts slightly tightened. Moreover, a scotch is applied on the lateral surface to prevent radial ejection of the hollow spheres. The whole projectile/specimen system is shown in Figure 4. Such an experimental setup is equivalent to a classical projectile-fixed target perforation test with a perforator of the same mass as that of projectile in our test. Indeed, the loss of velocity of the perforator in a classical perforation test is compensated by the velocity loss of our specimen-flying support system.

Figure 4. Photograph of the projectile/specimen system

With this experimental setup, the strain impulse $\varepsilon(t)$ recorded with the pressure bar permits to calculate the force and particle velocity at the measuring point with a one-dimensional elastic wave propagation theory (Eqn. 1).

$$\begin{aligned} F(t) &= S_b.E_b.\varepsilon(t) \\ v(t) &= C_b\varepsilon(t) \end{aligned} \qquad (1)$$

where S_b ,E_b, C_b are respectively the cross sectional area, the elastic modulus and the elastic wave speed of the pressure bar.

Such a measurement can be time shifted to the contacting/piercing end of the pressure bar with a careful data processing which takes the dispersion correction and the exact time shift setting into account [15-17]. Finally, this shifted force and velocity $F(t), v(t)$ is the piercing force time history and moving velocity of the piercing end.

The initial velocity of the launched sandwich specimen before the impact is also available, measured with two optical barriers. With this initial impact velocity, the velocity time-history

$v_{projectile}(t)$ of the projectile/specimen system can be evaluated by the deceleration due to the piercing force measured by pressure bar.

$$v_{projectile}(t) = V_0 - \int_0^t \frac{F(\tau)}{M} d\tau \qquad (2)$$

where M is the sum of the mass of the sandwich sample and that of the projectile.

The relative displacement time history is then calculated by equation 3.

$$U(t) = \int_O^t (v_{projectile}(\tau) - v(\tau)) d\tau \qquad (3)$$

In this way, accurate force-displacement curves under impact loading can be found.

Quasi-static tests are also performed using a universal testing machine to study the loading rate effect on the sandwich perforation. In order to have the same experimental condition, the same tube-like sample support as that in the impact perforation test is used here. A steel rod with the same diameter 16 mm and with the same semi-sphere 'nose' is used as the perforator (Figure 5).

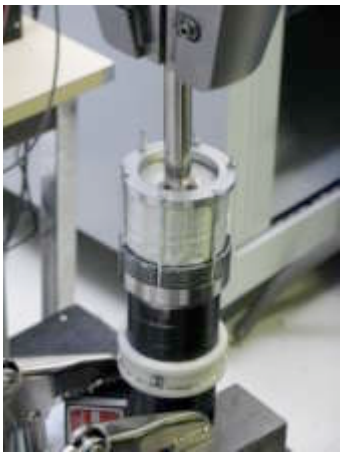

Figure 5. Photography of quasi-static set up.

A natural inquiry concerns the significance of such a test where the clamping boundary diameter is rather small with respect to the diameter of the perforator. For a similar sandwich plate with aluminium foam core, results under quasi static loading obtained with present experimental setup is compared with perforation tests with same perforator but on a 100x100mm clamping system, the peak loads are very close to each other [14]. Actually, the

clamping condition is well respected and the tested sandwich plate is rather rigid so that the perforation process is rather localised in a small area.

3 Experimental perforation of sandwich samples

In order to avoid any interaction between the wave propagation effect in the specimen and the breaking of the top skin of those sandwich plates, the impact velocity is chosen in the manner that the breaking of the top skin will occurs before the reflected wave comes back from the bottom skin. For this purpose, an impact velocity of 45m/s is prescribed for all of our tests, which corresponds to an average nominal strain rate of about 1000/s.

3.1 Perforation of sandwich plates with homogeneous cores

The inversed perforation tests at 44 m/s and under quasi-static loading are performed for the sandwich samples of the four homogeneous cores (S-C1 to S-C4). Experimental piercing force displacement curves are shown in figure 6.

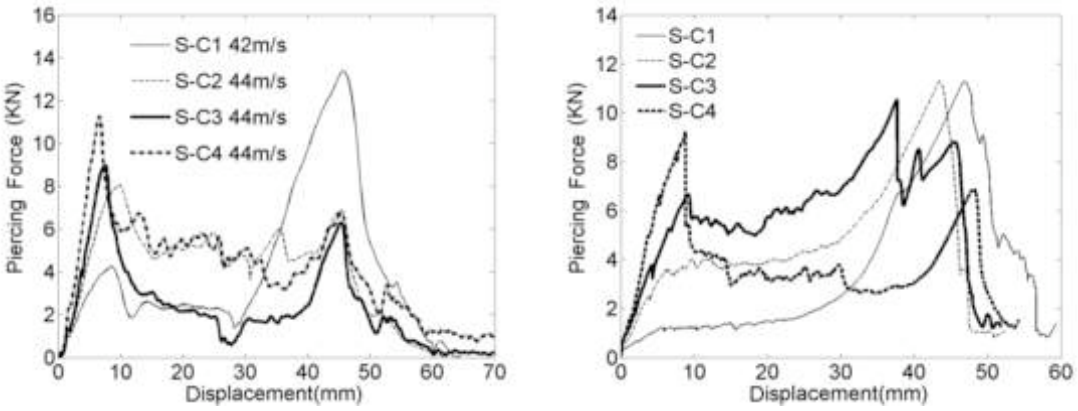

(a) (b)

Figure 6: Piercing force vs displacement curves for homogenous sandwich under impact (a) and static (b) loadings

From the impact perforation curves (Figure 6a), it can be seen that the perforation behaviour of sandwich samples depends strongly on the strength of their core (Table 2). For higher density cores as S-C2, S-C3 and S-C4, there are two distinct force peaks corresponding to the successive perforations of the two skin sheets. The first force peak (corresponding to the perforation of the incident top skin sheet) increases with the density of the core. The second force peak (bottom sheet) is independent of core density (table 2) which is believed to be the piercing force for skin sheet alone. For the weakest core S-C1, the curve is rather

different with a first peak lower than the aforementioned piercing force of a skin sheet alone. Actually, the post-mortem observation shows that the incident skin sheet is not perforated in the case of S-C1.

Sandwiches	S-C1	S-C2	S-C3	S-C4
Core Density (Kg/m^3)	156	242	343	468
The first force peak (N)	-	8072	8978	11249
The second force peak (N)	-	6896	6301	6781

Table 2. Impact piercing force peaks of the incident top skin and the bottom skin

The same conclusion is also made from quasi static tests. For weaker core materials (S-C1 and S-C2), no perforation of the top skin sheet is observed. For the stronger core materials, the top skin piercing force increases with the strength of the core. As the core material strength is enhanced at impact loading rate at about 10% [8] (because of the base material rate sensitivity), the top skin of sandwich S-C2 not perforated under static loading is finally perforated under impact loading. To illustrate this viewpoint, a comparison between the static and impact perforation curves for the sandwich sample S-C4 shows that the first peak as well as perforating force within the core are enhanced (Figure 7).

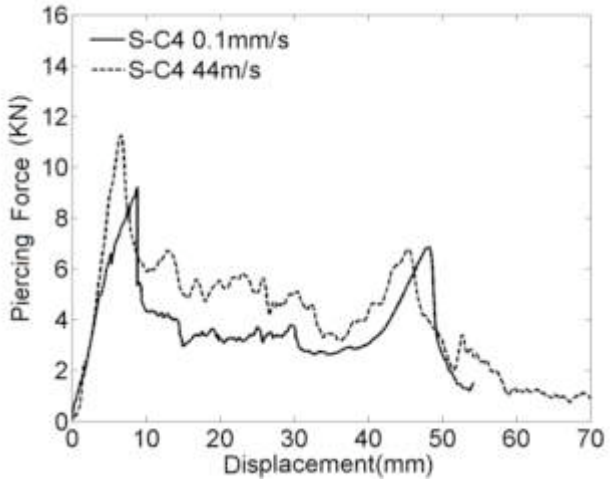

Figure 7 Comparison between quasi-static and impact perforating force for sandwich S-C4.

3.2 Perforation of sandwich plate with graded cores

Figure 8 shows the force-displacement curves of graded core sandwich perforation for the two gradient profiles. The tests are perfectly repeatable which shows the quality of the sample with the gradient profiles.

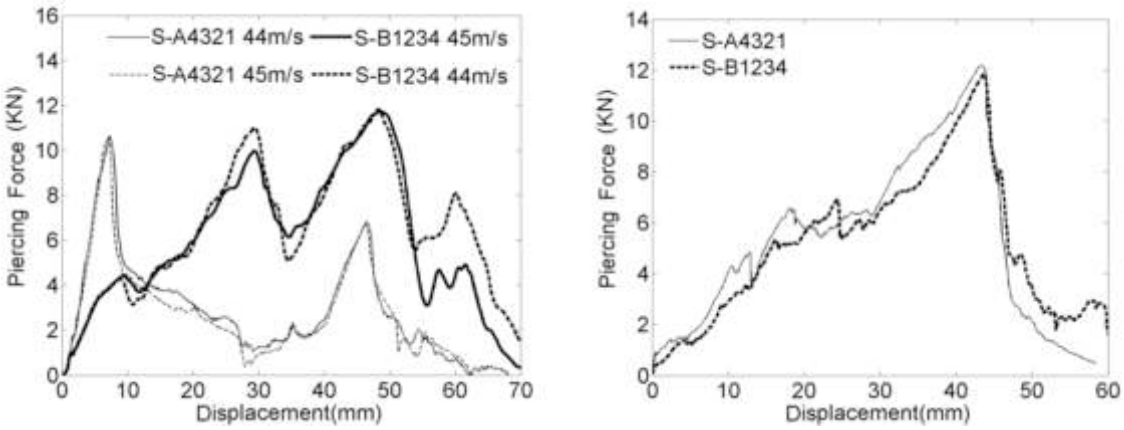

(a) (b)

Figure 8. Piercing curves of sandwich with graded cores at 45m/s (a) and at quasi-static loading (b)

On the one hand, the gradient profiles play a very important role under impact loading and the force displacement curves differ very sharply. For S-A4321, the results show the two force peaks for the two successive top and bottom skin sheets breaking. For S-B1234, the top skin sheet was not perforated before 20mm displacement (half way) because of the low force level. Actually, the post-mortem examination (Figure 9) shows that the incident top skin only folds and never breaks (Fig. 9c).

(a) (b)

(c) (d)

Figure 9 Post-mortem observations of the top and bottom skins for S-A4321 (a),(b) and S-B1234 (c) and (d).

On the other hand, it is clear that the gradient profiles have no influence on the quasi-static perforation (Fig. 8b). It may indicate that the perforation process for the two gradient profiles is the same. The post-mortem observations show also a folding process is dominant for the two gradient profiles (Figure 10).

Figure 10 Post mortem photos sandwichs under quasi-static perforation

An interesting suggestion is that the first layer of the core is the governing feature of the perforation process under impact loading. Indeed, the comparison proposed in figure 11 reveals the similarities between S-A4321 and S-C4 and also between the profile B1234 and S-C1.

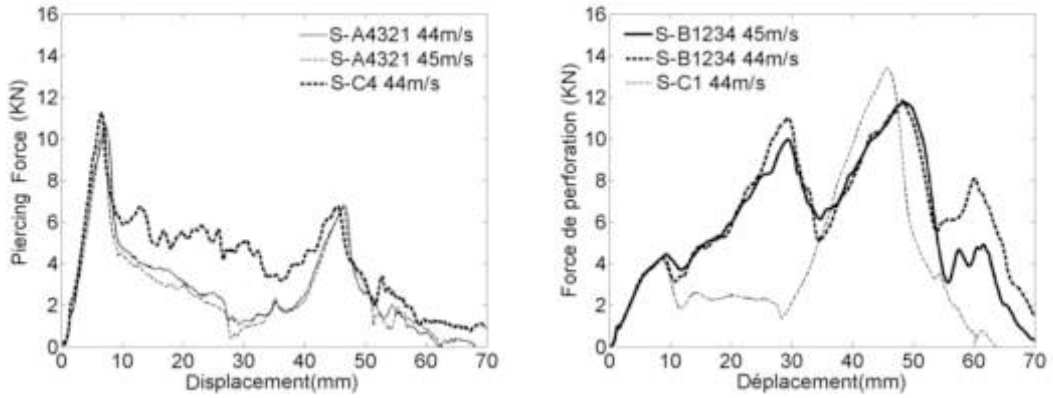

Figure 11. Comparisons (a) between graded core S-A4321 and homogeneous core S-C4 and (b) S-B1234 with S-C1.

Another interesting feature is the energy absorption capacities in the two cases. We define the absorbed energy for the dynamic perforation by using the following equation (4):

$$E(u) = \int_0^U F du \tag{4}$$

where u is the penetrating displacement, and F the measured force on the pressure bar.

This energy absorption as well as specific energy per mass is plotted in Figure 12 for the two gradient profiles A4321 and B1234. It shows that the best strategy lies in avoiding the piercing of the incident skin sheet so that this sheet deforms inside the core material which is a highly energy consuming process. Such a goal is easily reached by putting a weak layer under the incident skin sheet as the gradient profile B1234.

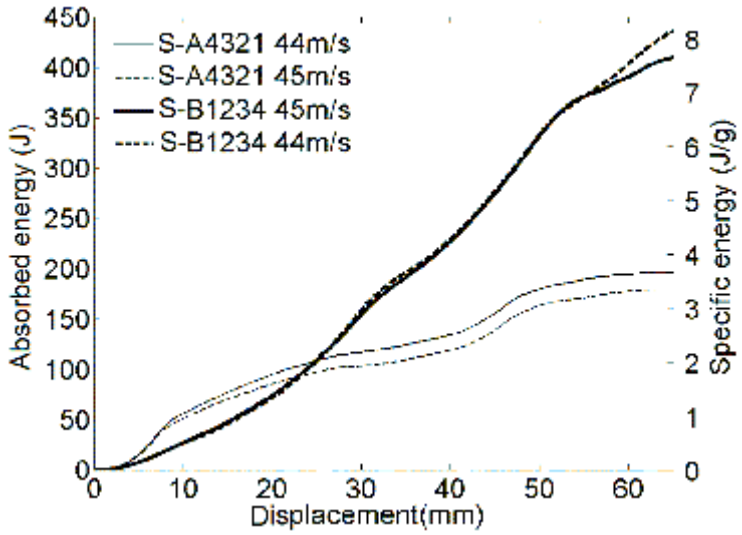

Figure 12. Energy absorption during piercing process .

4. Numerical simulations and analyses

The experimental results confirm the influence of the gradient profiles on the perforation process under impact loading and reveal the importance of the first layer of the core. However, as there is no detailed local information due to experimental difficulties, numerical analysis is proposed to make a virtual test and to understand the perforation process of sandwich with graded cores.

4.1 Numerical model

The numerical model of the graded sandwich consists of two skins of aluminium and the graded core. The graded core contains four layers with different densities.

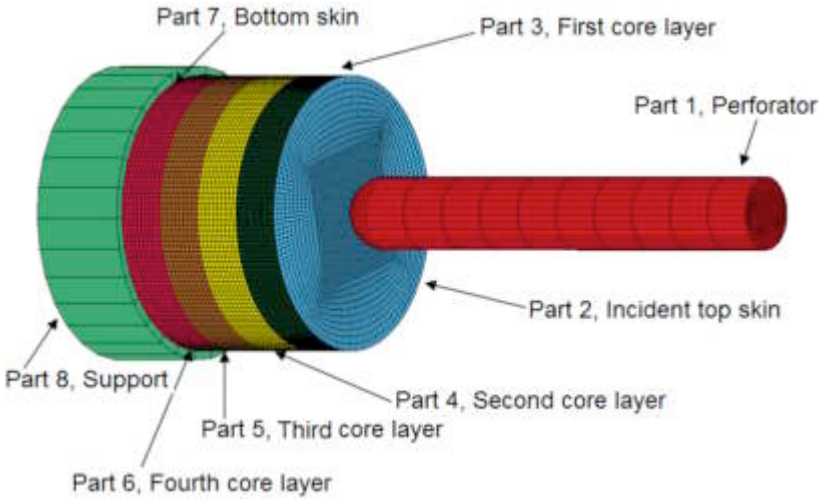

Figure 13 Numerical model for the perforation of a sandwich sample

The numerical model consists of 8 parts using explicit code LS-DYNA (Ls-971 version) as shown in Figure 13. As the most important zone is the first layer, 128.000 8-nodes cubic elements is used in the first layer, which is 4 times more than the other layers.

The behaviour of the skin sheet is modelled by a damageable isotropic hardening elastic-plastic constitutive law, available in Ls-Dyna as the model of type 104 (MAT_DAMAGE_1) [18]. The parameters used for 2024 T3 aluminium sheet were identified from normalised tension tests [2].

The behaviour of the core is represented by the material model of type 154 (MAT_DESHPANDE_FLECK_FOAM), which gives the relation between an equivalent stress and an equivalent strain depending on a criterion shape parameter α [18,19]. The

equivalent stress and strain relation available in Ls-Dyna is an empirical one (Equation 5) with γ, α_2 and β as the fitting parameters [2,18].

$$\sigma_Y = \sigma_{pl} + \gamma\hat{\varepsilon}/\varepsilon_D + \alpha_2 \ln\left(\frac{1}{1-(\hat{\varepsilon}/\varepsilon_D)^{\beta}}\right) \quad (5)$$

where σ_{PL} is the flow stress, ε_D is defined as the locking strain.

These parameters are identified for the four hollow spheres with the density C1-C4 by curve fitting with experimental results of uniform compression [8]. They are listed in table 3.

	C1	C2	C3	C4
ρ (kg/m^3)	156	242	343	468
E (MPa)	6.7	32.65	110.39	169.31
V	0	0	0	0
A	2.12	2.12	2.12	2.12
σ_{Pl}(MPa)	0.8	2.95	5.5	8
γ (MPa)	0.95	0.99	1.23	6.05
α_2(MPa)	20.4	21.2	19.3	21.7
B	3.7	9.1	9.5	5.3
ε_D	1.7	1.57	1.4	0.9018
$\boldsymbol{\varepsilon_{cr}}$	0.1	0.1	0.1	0.1

Table 3. Identified parameters of Fleck model.

The perforation simulation is realized by applying a prescribed initial velocity (45m/s as in a real test) to the specimen and the flying support.

The quality of this numerical model is verified with the simulation of the perforation of homogeneous sandwich samples S-C1 to S-C4 (four layers with the same material parameter set). Figure 14 illustrates that the simulations can catch the main testing features at the early stage around the first peak. However, such model cannot catch the piercing feature within the cores after this early stage (about 10mm perforation). The reason that this numerical model failed to catch the reality after the early stage lies in the bad representation of foam like materials by the used constitutive model in a shear dominant loading. Indeed, the used constitutive law is based on the equivalent stress strain relationship and the parameters are only determined by the compression results. It is not really surprising that it does not work in a shear dominant situation. However, our main focus is on the top skin breaking which determine the whole perforation process so that the present numerical model is sufficient to reproduce this feature.

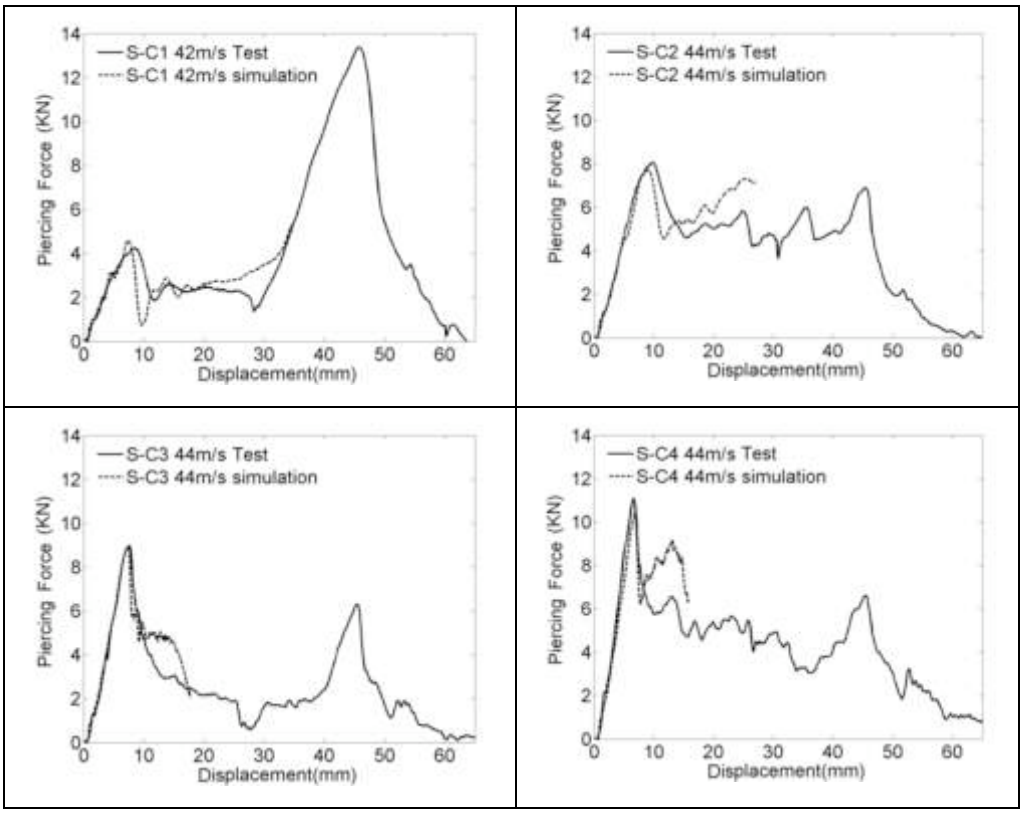

Figure 14 Comparison between the test and the simulation for the homogenous sandwich.

4.2 Impact perforation simulations for sandwich plates with graded core

For S-A4321 sandwich, the simulated force-displacement curves as well as the experimental ones are shown in Figure 15a. They correspond perfectly till about 10mm displacement where the incident skin is broken and significant perforation of the core begins. This indicates again that the used material law and the erosion rule for core materials do not allow for a reasonable accuracy in a shear dominant loading state.

As to the S-B1234 sandwich, the simulated curve follows also the experimental curve till about 10mm perforation (Figure 15b). Afterwards, as there is no top skin sheet breaking, the simulated results can still catch the main feature till 20mm.

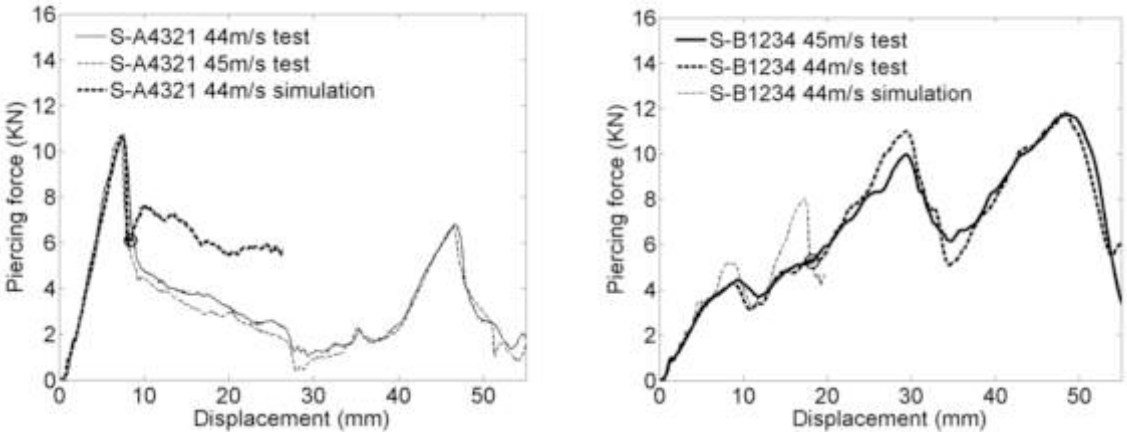

(a) (b)

Figure 15 Comparisons between tests and simulations for graded core sandwich plates S-S-A4321 (a) and S-B1234 (b) under impact loading.

From these simulated tests, it is easy to study the deforming map of each layer at any time. The deforming states at about 10mm perforation for S-A4321 (marked by a ring in Figure 15) and states at about 20mm perforation for S-B1234 are compared in figure 16. For S-A4321 (Fig.16a), it reveals that there is no significant global deformation of the cores from the lateral external viewpoint. The piercing is rather localised under the perforator in this case. For S-B1234 (Fig.16b), it can be seen that there is no perforation of the top skin and the weaker first layer are nearly all crashed.

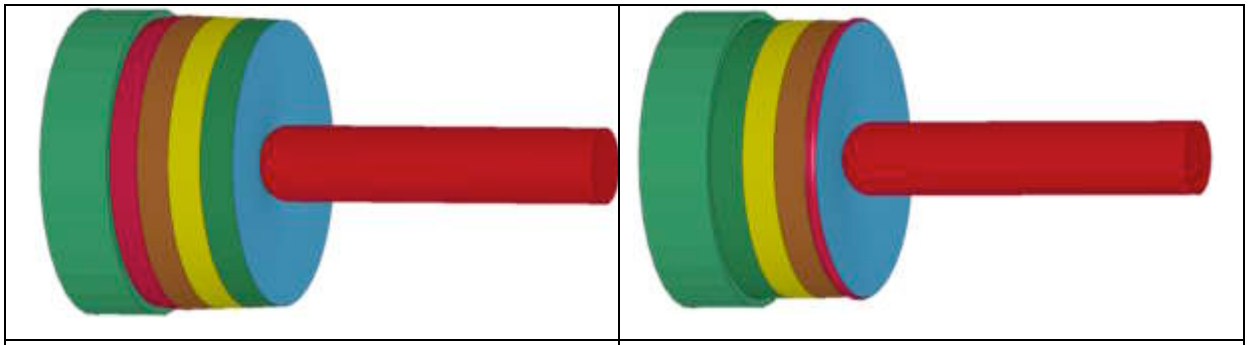

(a) (b)

Figure 16 The deforming map for S-A4321(a) and S-B1234 (b) dynamic loading.

In order to show the evolution of deformation in each layer, a normal strain in each layer is defined as the ratio of the actual thickness at the centre of each layer over their initial thickness. Such time-history of nominal strain in each layers are plotted in Figure 17 for S-A1234 as well as B-1234. It could be seen that the deformation is concentrated in the first

layer and its strength determines if the top skin will be perfored or not. Such results confirm the dominant role played by the first layer just in contact with the top skin.

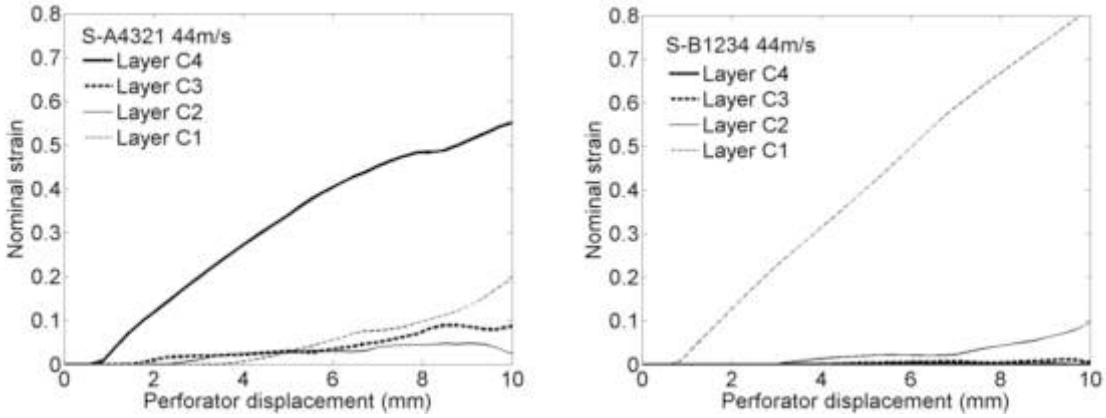

(a) (b)

Figure 17 Nominal strain evolution for S-A4321(a) and S-B1234 (b) dynamic loading.

2.3 Quasi-static perforation simulation for sandwich plates with graded core.

The deforming map of graded sandwich under quasi-static loading is also interesting. As the material model of type 154 *(MAT_DESHPANDE_FLECK_FOAM) is not available in implicit version, the quasi-static simulation is realized with the "mass scaling" method. The boundary condition in the quasi-static simulation is the following: the support is fixed in all degrees of freedom and the perforator pushes with a constant velocity of 0.1mm/s.

Figure 18 shows the results of the perforation simulations of graded sandwich S-A4321 and S-B1234 under quasi-static loading. The simulation matches also the main feature of experiments.

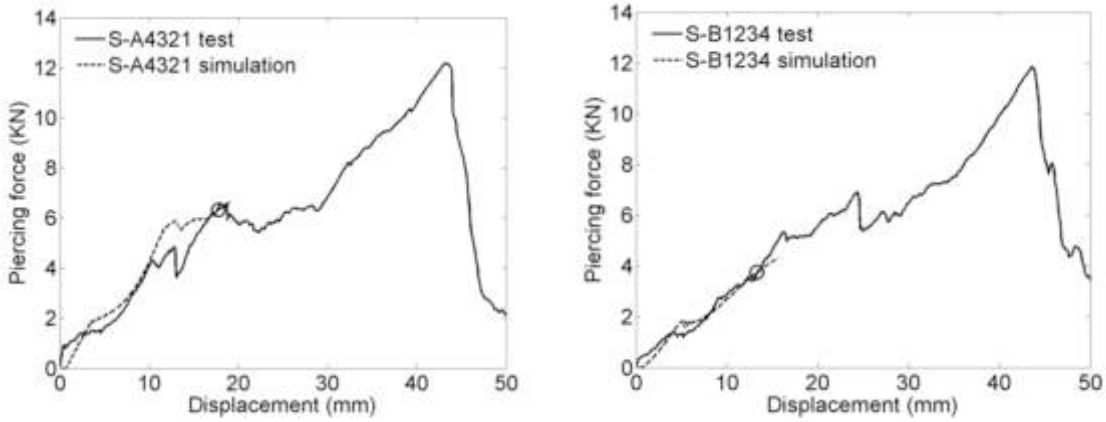

(a) (b)

Figure 18 Comparisons between tests and simulations for graded core sandwich plates S-S-A4321 (a) and S-B1234 (b) under quasi-static loading.

In contrast to the case of impact perforation of the same graded sandwich S-A4321 (Figure 17a), there is no perforation of the top skin sheet even if the hardest layer is placed just under the top skin. This is because of the equilibrium state that should be reached in a quasi-static test. Thus, wherever the weak layer is placed, if its strength is lower than the piercing force of the skin sheet, the top skin breaking will not occur. In Figure 18, it can be seen that from nominal strain evolution in both S-A4321 and S-B1234, the weakest layer takes always the main part of the deformation.

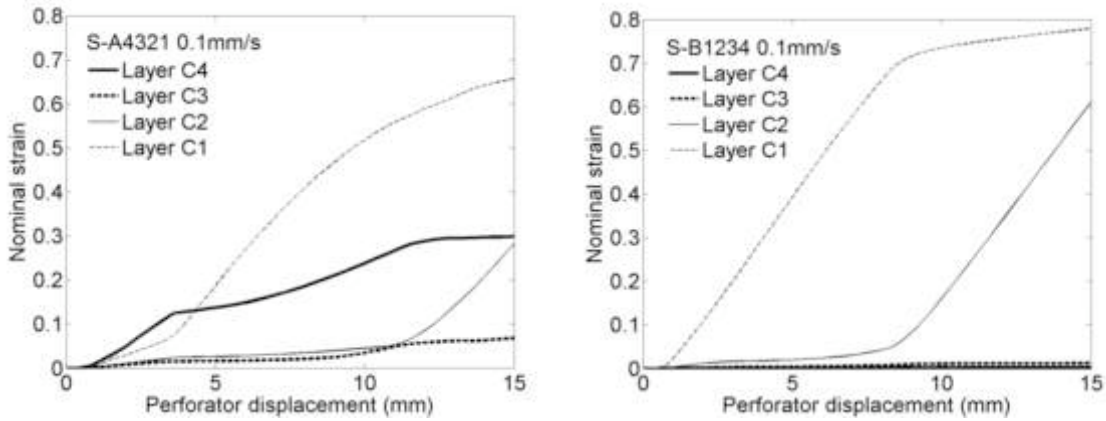

(a) (b)

Figure 18 Nominal strain evolution for S-A4321(a) and S-B1234 (b) quasi-static loading.

5 Conclusion

The inverse perforation testing technique with a long thin instrumented Hopkinson bar is successfully applied to the measurement of piercing forces during the whole perforation process of sandwich samples made of aluminium skins and polymeric hollow sphere cores (with or without a gradient profile). Quasi-static tests using the same clamping device provide a comparison between impact piercing force-displacement curves and the static ones.

Preliminary testing results on the sandwich sample with homogeneous core (without density gradient) show that there is no significant loading rate effect in the perforation process under moderate loading speeds (around 45m/s). The governing parameter is the ratio between the strength of the core materials (could be enhanced under impact loading) and the piercing force of aluminium skin sheet. Thus, if the core material strength is greater than this piercing

force, the skin sheet breaks and perforator makes a hole in the core afterwards. Otherwise, the core crushes and the skin sheet folds into the core and this is a much more energy consuming process.

For the sandwich with a property gradient, in addition of experimental observation, the simulation of all the tests using Ls-Dyna explicit code allows for a detailed deforming map at any time position for further understanding. The main features are the following: under static loading, the ratio of the strength of the weakest layer with respect to the skin sheet piercing force determines if the top skin will break or not. Under moderate impact loading, the perforation process is governed by the ratio of the strength of the first layer just under the incident skin sheet with respect to the skin piercing force. The gradient profile has thus a large influence on the impact perforation behaviour of the sandwich samples. A weaker first layer (than the piercing force of skin sheet) under the incident skin sheet and a progressively enhanced core is suggested to avoid the skin sheet breaking and to favour a highly energy consuming process by folding the top skin into the core material.

Acknowledgement

The authors recognize and acknowledge the European network of Excellence, KMM-NoE, for the financial support of the presented work.

Reference

[1] Gibson L.J., and Ashby M., Cellular solids. Pergamon Press, 1988.

[2] Hanssen A.G., Girard Y., Olovsson L., Berstad T., Langseth M., A numerical model for bird strike of aluminium foam-based sandwich panels, International Journal of Impact Engineering, in press.

[3] Suresh S., Mortensen A., 1998. Fundamentals of Functionally Graded Materials. The Institute of Materials, London.

[4] Li T., Ramesh K.T. and Chin E.S.C, Dynamic characterization of layered and graded structures under impulsive loading. International Journal of Solids and structures 38 (2001), 6045–6061.

[5] Gupta N., A functionally graded syntactic foam material for high energy absorption under compression. Materials Letters 61 (2007), 979–982.

[6] Apetre N.A., Sankar B.V., and Ambur D.R., Low-velocity impact response of sandwich beams with functionally graded core. International Journal of Solids and Structures 43 (2006), 2479–2496.

[7] Sanders W.S., Gibson L.J., Mechanics of hollow sphere foams. Materials Science and Engineering C347 (2003), 70–85.

[8] H.B.Zeng, S.Pattofatto, H.Zhao, Y.Girard and V.Fascio, Impact behaviour of hollow sphere agglomerates with density gradient, International Journal of Mechanical Science, In press.

[9] Li Y., Li J.B, Zhang R.Q., Energy-absorption performance of porous materials in sandwich composites under hypervelocity impact loading, Composite Structures 64 (2004) 71–78

[10] Mines, R.A.W, Worrall C.M, and Gibson, A.G., Low velocity perforation behaviour of polymer composite sandwich panels. Int. J. Impact Engng, 21 (1998), 855–879.

[11] Hoo Fatt M.S, Park K.S., Perforation of sandwich plates by projectiles. Composites: Part A: applied science and manufacturing 31 (2000), 889-899.

[12] Tien-Wei Shyr, Yu-Hao Pan, Low velocity impact responses of hollow core sandwich laminate and interply hybrid laminate, Composite Structures 64 (2004) 189–198

[13] Wierzbicki T, de Lacruz-Alvarez A, Hoo Fatt MS, Impact energy absorption of sandwich plates with crushable core. In: Proceedings of the ASME/AMD Symposium, Impact Waves, and Fracture. Los Angeles, CA, June 1995;205:391–411.

[14] H.Zhao, I.Elnasri, Y.Girard, Perforation of aluminium foam core sandwich panels under impact loading –An experimental study, *Int.J.Impact Engng.* 34(2007),1246-1257.

[15] Gary G., Klepaczko J.R, Zhao H., Correction de dispersion pour l'analyse des petites déformations aux barres de Hopkinson, Journal of Physique 1 (1991), C1, 403-410.

[16] H.Zhao, G.Gary, Une nouvelle méthode de séparation des ondes pour l'analyse des essais dynamiques. *C.R. Acad. Sci. Paris.* **319** (1994), série II, 987-992.

[17] H.Zhao, G.Gary, Behaviour characterisation of polymeric foams over a large range of strain rates, *Int. J. vehicle design*, **30** (2002), 135-145.

[18] Hallquist J.O., Ls-Dyna theoretical manual. Livermore Software Technology Corporation, 1998.

[19] Deshpande V.S and Fleck N.A, Isotropic constitutuve models for metallic foams, Journal of the Mechanics and Physics of Solids 48 (2000), 1253-1283.